

## Phenomenon of Alfvénic Vortex Shedding

M. Gruszecki,\* V. M. Nakariakov, T. Van Doorsselaere, and T. D. Arber

*Centre for Fusion, Space and Astrophysics, Department of Physics, University of Warwick, Coventry CV4 7AL, United Kingdom*  
(Received 14 May 2010; published 30 July 2010)

Generation of Alfvénic (magnetohydrodynamic) vortices by the interaction of compressible plasma flows with magnetic-field-aligned blunt obstacles is modeled in terms of magnetohydrodynamics. It is found that periodic shedding of vortices with opposite vorticity is a robust feature of the interaction in a broad range of plasma parameters: for plasma beta from 0.025 to 0.5, and for the flow speeds from 0.1 to 0.99 of the fast magnetoacoustic speed. The Strouhal number is the dimensionless ratio of the blunt body diameter to the product of the period of vortex shedding and the inflow speed. It is found to be consistently in the range 0.15–0.25 in the whole range of parameters. The induced Alfvénic vortices are compressible and contain spiral-armed perturbations of the magnetic field strength and plasma mass density up to 50%–60% of the background values. The generated electric current also has the spiral-armed structuring.

DOI: [10.1103/PhysRevLett.105.055004](https://doi.org/10.1103/PhysRevLett.105.055004)

PACS numbers: 52.30.Cv, 52.35.We, 52.65.Kj, 95.30.Qd

It is well known that the interaction of a flow with a nonmoving bluff body results in a so-called *Kármán vortex street*, where vortices with opposite vorticity are periodically generated alternating from either side of the blunt body in the downstream region, e.g. [1,2]. The phenomenon of periodic shedding of hydrodynamic vortices has many consequences in oceanography, atmospheric physics and engineering. The phenomenon can be considered as an example of auto oscillations, when a steady energy supply causes an oscillatory behavior of the dynamical system.

The effect of vortex shedding in a magnetized medium is less well understood. It is known to play a role in a number of applications and physical situations. For example, in industrial magnetohydrodynamics (MHD) the effect of MHD vortex shedding can be used for the leveling the temperature by convective transport in liquid metals, e.g., [3]. In controlled fusion, this effect is studied in association with the formation of coherent structures (blobs) in the scrape-off layer of tokamak plasmas [4]. In geophysics, the observed rocking of the floating bubbles in the equatorial ionospheric *F* region is attributed to this effect [5]. Similarly, a zigzag path of magnetic flux tubes emerging in the solar interior, caused by vortex shedding, has been found in numerical simulations [6]. Also, this effect has been found to accompany the impulsive plasmoid penetration of the magnetosphere [7]. Also, the size of the vortices generated by the interaction of the solar wind with Earth is important in the context of the solar-wind–magnetosphere coupling [8]. Strong vortex shedding has been observed coincident with disruption and reformation of the termination shock in MHD simulations of astrophysical jets [9]. There is a growing interest to Alfvénic vortices and their generation in the magnetopause and magnetosheath, e.g., [10,11]. Recently, periodic shedding of MHD vortices was suggested as a mechanism for the excitation of kink oscillations of plasma loops in the solar corona [12].

The quantitative characteristics of the vortex shedding phenomenon is the Strouhal number that is a dimensionless parameter constructed from the period of the vortex shedding, the size of the blunt body and the flow velocity. In hydrodynamics, the typical value of the Strouhal number that describes the interaction of a steady flow with a cylindrical obstacle of a circular cross-section is in the range from 0.15 to 0.2 [2]. In magnetized fluids and plasmas, there has not been a systematic and detailed studies of this parameter. Its value and dependence upon the physical parameters (such as plasma-beta, flow speed, size of the blunt body) is important for the development of diagnostic techniques and interpretation of observed phenomena, discussed above. In some studies the Strouhal number has been estimated. For example, in the numerical experiments on the magnetohydrodynamic flows of liquid metals [3] the Strouhal number was found to be about 0.2. In the Earth's magnetospheric plasma, the Strouhal number has experimentally been estimated as 0.3 [13]. Theoretically, in the case of MHD, the consideration of the plasma motion in the plane perpendicular to the magnetic field is governed by the gradients of the total, magnetic and gas, pressure. These pressures have different dependence upon the mass density. In the adiabatic case the gas pressure is proportional to the density to the power of  $\gamma = 5/3$ , while the magnetic pressure depends upon the density squared. Thus, the consideration of the MHD flows requires both terms are explicitly included; i.e., it can not be determined from a simple rescaling of results from nonmagnetized fluid [14].

The aim of this Letter is to present the parametric numerical study of the interaction of a steady plasma flow with a cylindrical obstacle in the MHD regime, and to determine the dependence of the Strouhal number upon the plasma properties.

Our governing equations are the compressible magnetohydrodynamic (MHD) equations,

$$\frac{\partial \varrho}{\partial t} + \nabla \cdot (\varrho \mathbf{V}) = 0, \quad (1)$$

$$\varrho \frac{\partial \mathbf{V}}{\partial t} + \varrho (\mathbf{V} \cdot \nabla) \mathbf{V} = -\nabla p + \frac{1}{\mu} (\nabla \times \mathbf{B}) \times \mathbf{B}, \quad (2)$$

$$\varrho \frac{\partial \varepsilon}{\partial t} + \varrho \mathbf{V} \nabla \varepsilon = -p \nabla \cdot \mathbf{V}, \quad (3)$$

$$\frac{\partial \mathbf{B}}{\partial t} = \nabla \times (\mathbf{V} \times \mathbf{B}), \quad (4)$$

$$\nabla \cdot \mathbf{B} = 0, \quad (5)$$

where  $\varrho$  is the mass density,  $p$  is the gas pressure,  $\mathbf{B}$  is the magnetic field,  $\mathbf{V} = [V_x, V_y, V_z]$  is the flow velocity; and  $\mu$  is the magnetic permeability and  $\varepsilon$  is the specific internal energy density,  $p = \varrho \varepsilon (\gamma - 1)$  and  $\gamma = 5/3$  is the ratio of specific heats. Some potentially important effects, e.g., dispersion and drift multifluid effects, are missing in the governing equations. The initial characteristic spatial scales of the vortices are much larger than all relevant kinetic scales; hence, the application of the MHD equations is well justified.

We consider an equilibrium which corresponds to the interaction of an initially uniform and steady plasma flow with a cylindrical blunt body. The axis of the cylinder is chosen in the  $y$  direction. Initially, both plasma pressure and the magnetic field are uniform over the whole space around the blunt body to keep pressure balance. Thus, the initial, equilibrium plasma quantities are  $(p(x, z), \varrho(x, z), B\hat{y}) = (p, \varrho, B)$  in  $x^2 + z^2 > d^2/4$ , where  $\hat{y}$  is the unit vector of the  $y$  axis and  $d$  is the diameter of the cylinder. The magnetic field is directed along the  $y$  axis, parallel to the blunt body axis. To initiate of vortex shedding everywhere outside the cylinder we set homogeneous flow in the  $x$  component of velocity  $V_x$ . To exclude effects of cylinder deformation, instability, and motion along the  $x$  direction the cylinder is treated as a rigid body, i.e.,  $\mathbf{V}(x, z) = 0$  everywhere inside  $x^2 + z^2 < d^2/4$ . The specific quantitative values of the initial equilibrium are taken to be consistent with the typical parameters of the solar coronal plasma (see Table I). However, the results obtained can be easily applied to other relevant plasma systems by straightforward renormalization.

Eqs. (1)–(5) are numerically solved with the use of the Lagrangian-remap code LARE2D [15]. LARE2D operates by taking a Lagrangian predictor-corrector time step and after each Lagrangian step all variables are conservatively remapped back onto the original Eulerian grid using Van Leer gradient limiters. The code was designed for the simulation of nonlinear dynamics of low  $\beta$  (the ratio of the gas pressure to the magnetic pressure) plasmas with steep gradients. The magnetic field  $\mathbf{B}$  is defined on cell

faces and is updated with constrained transport to keep  $\nabla \cdot \mathbf{B} = 0$  to machine precision. We simulate the plasma dynamics in a domain  $(-50, 50) \times (-25, 25)$  Mm covered by  $6500 \times 2500$  grid points, with the field-aligned cylindrical body being situated at the point  $(0, 0)$ . We performed grid convergence studies to check the numerical results. We set zero gradients boundary conditions at all sides of the simulation box, allowing a propagating perturbation signal to leave freely, without reflection. Figure 1 shows a typical snapshot of the von Kármán vortex street, generated by the interaction of the steady flow with the cylinder situated at the  $(0, 0)$  point. The phenomenon of vortex shedding is clearly seen: vortices of the opposite vorticity  $\omega = \nabla \times \mathbf{V}$  are alternatively and periodically generated on the opposite sides of the blunt body and then dragged with the flow downstream. The generated flow vorticity is parallel to the magnetic field.

We performed a series of numerical experiments, studying the effects of the cylinder diameter, plasma parameter  $\beta$  and the steady flow speed on the phenomenon. Both sub-Alfvénic and super-Alfvénic speeds were considered, while in all cases the flow speed remained lower than the fast magnetoacoustic speed. When the flow speed exceeds the characteristic speed of the information transfer across the magnetic field in the plasma, the fast magnetoacoustic speed,  $(c_s^2 + V_A^2)^{1/2}$ , the interaction changes qualitatively, as the shocks are formed. The latter regime is not considered in this study.

Figure 2 shows the dependence of the Alfvénic vortex shedding period  $P$  upon the flow speed  $V_0$  for different diameters  $d$  and the plasma  $\beta$  ranging from 0.025 to 0.5. The variation of plasma  $\beta$  is achieved by the altering plasma pressure. One of the aims of this study is to test the hydrodynamic relation,

$$\frac{d}{PV_0} = \text{St}, \quad (6)$$

where the constant  $\text{St}$  is the Strouhal number in the MHD regime. The dependence of the Strouhal number, calculated according to Eq. (6) upon the flow speed is shown in

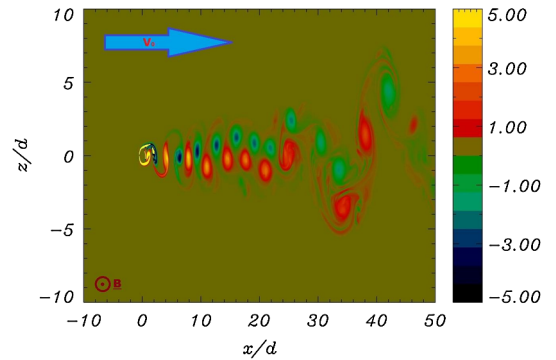


FIG. 1 (color online). Normalized profile of the vorticity  $\omega = \nabla \times \mathbf{V}$  at  $t = 220$  s for the case of the  $V_0 = 0.3$  Mm/s. Spatial coordinates  $x$  and  $z$  are measured in units of diameter of the cylinder  $d = 1$  Mm. The value of vorticity  $\omega$  is measured in the units of  $d/V_0$ .

TABLE I. Parameters of the initial numerical equilibrium.

$\varrho_0$ [kg/m <sup>3</sup> ]	$p_0$ [Pa]	$B_0$ [T]	$T_0$ [K]	$c_s$ [Mm/s]	$V_A$ [Mm/s]	$\beta$
$10^{-12}$	$10^{-2}$	$10^{-3}$	$6 \times 10^5$	0.129	0.892	0.025

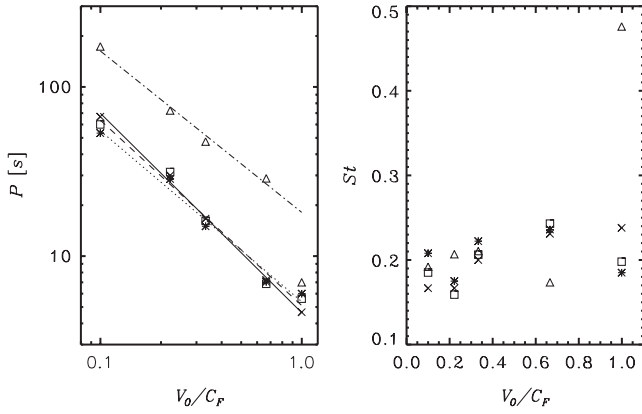


FIG. 2. The variation of the period  $P$  of Alfvénic vortex shedding (left panel) and the Strouhal number  $St$  (right panel) with the incoming flow speed  $V_0$ . The speed is measured in units of the equilibrium fast magnetoacoustic speed  $C_F$ . The stars shows the results obtained for the cylinder with diameter  $d = 1$  Mm, and the triangles for  $d = 3$  Mm, and  $\beta = 0.025$ ; the squares and crosses corresponds to  $\beta = 0.1$  and  $\beta = 0.5$ , respectively, for  $d = 1$  Mm. The gradients of the best-fitting straight lines are  $-1.17$  (solid line),  $-1.01$  (dotted line),  $-1.1$  (dashed line) and  $-0.95$  (dash-dotted line).

the right panel of Fig. 2. In the calculations, the power-law dependence of the period upon the speed was determined by best fitting the experimental dependence in the log-log plot with a linear function, using the least-square method (Fig. 2, left panel). The gradients of the approximating straight lines for all combinations of the parameters are found to be close to  $-1$ , hence  $\log P \propto -\log(V_0)$ . Thus, the scaling given by Eq. (6) is confirmed to take place in the MHD regime. It is established that the Strouhal number is almost independent of the flow speed and is consistently in the range  $0.15$ – $0.25$ . Thus, the vortex shedding phenomenon can be considered as an example of self-organization of the system: the period of vortex shedding is determined by the blunt body diameter and the inflow speed. The coefficient of the proportionality of these values is the Strouhal number. The abnormal value of  $St$  corresponding to the flow speed of about unity in one of the experiments is attributed to flows locally exceeding the magnetoacoustic speed. The results are found to be independent of the plasma  $\beta$ .

Figure 3 shows time-distance signatures of the perturbed mass density  $(\varrho - \varrho_0)/\varrho_0$ , collected at  $x = 8$  Mm along the  $z$  axis from the instant of time when the first vortex is reaching the observational point. The vortices are clearly visible in the mass density perturbations. For all vortices we see decreases in density towards their centers (see also Fig. 5). The dependence of the extreme values of the perturbations of the mass density, and the absolute values of the magnetic field and electric current density in the generated von Kármán street upon the value of the incoming flow speed is shown in Fig. 4. The estimations are based upon the use of five vortices in the street. The decrease in the mass density of the plasma at the vortex center reaches

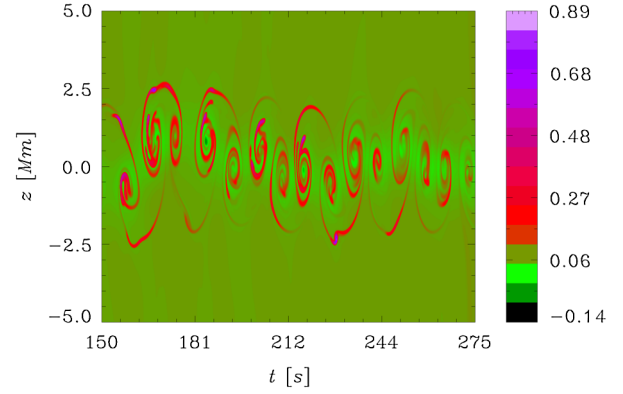


FIG. 3 (color online). Time-distance signatures of the normalized mass density variations in the generated street of Alfvénic vortices,  $(\varrho - \varrho_0)/\varrho_0$ , collected at  $x/d = 8$ .

about  $10\%$ . In the vortex periphery, the density is enhanced by up to  $50\%$ – $70\%$ . Thus, the vortices are essentially compressible. Hence, strictly speaking, they should be called as fast magnetoacoustic (see [17], for a detailed discussion). However, we shall keep using the established terminology and call them Alfvénic. The gas pressure perturbation, not shown here, exhibits a very similar shape.

The vortex diameter is measured as a distance between the points where the vorticity  $\omega$  was 2 times larger than in vortex center. To estimate it we used the vortex which reached the point  $x/d \approx 10$ . The size of the generated Alfvénic vortices is found to be the same order of magnitude as the size of the blunt body (Fig. 4, last panel), similar to hydrodynamics. Figure 5 shows zoomed contour plots of the internal structure of a vortex. The mass density and the magnetic field at the vortex center are decreased. The trans-

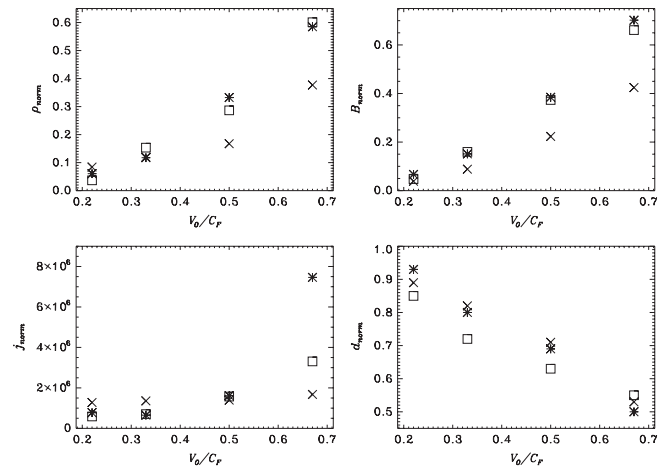


FIG. 4. Normalized minimum value of density  $\varrho_{\text{norm}} = |(\varrho - \varrho_0)/\varrho_0|$  (top left panel), minimum value of magnetic induction  $B_{\text{norm}} = |(B - B_0)/B_0|$  (top right panel), maximum value of electric current  $j_{\text{norm}} = j(d/B_0)$  (bottom left panel) and vortex diameter  $d_{\text{norm}} = d_{\text{vortex}}/d$  (bottom right panel) as functions of the flow speed. The speed is measured in units of fast speed  $C_F$ . The stars, squares and crosses corresponds to  $\beta = 0.025$ ,  $\beta = 0.1$  and  $\beta = 0.5$ , respectively.

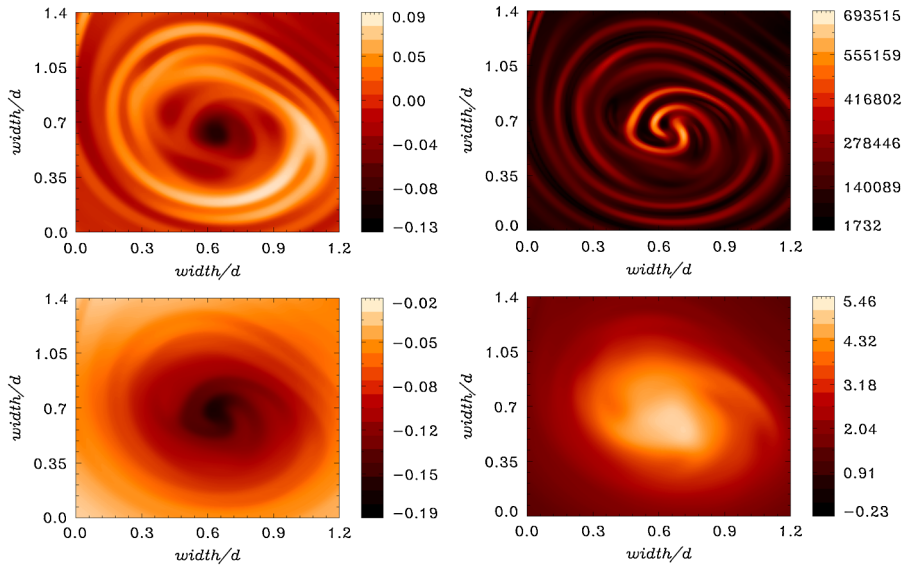


FIG. 5 (color online). Internal structure of an Alfvénic vortex: the mass density  $(\rho - \rho_0)/\rho_0$  (top left panel), the absolute values of the electric current density  $j(d/B_0)$  (top right panel), magnetic field  $(B - B_0)/B_0$  (bottom left panel) and vorticity  $\omega_{\text{norm}} = \omega \cdot d/V_0$  (bottom right panel).

verse gradients in the magnetic field generate the current density according to the Ampere's law  $\mathbf{j} = \nabla \times \mathbf{B}/\mu$ . The induced current is clearly filamented, with individual current sheets having the structure of spiral arms. Similar structuring is seen in the density, vorticity  $\omega = \nabla \times \mathbf{V}$  and the magnetic field. Generation of such filamentary arms have been also observed, e.g., in numerical experiments on the excitation of torsional Alfvén waves by a rapidly spinning rotor embedded in a magnetized plasma [16].

In conclusion, we have numerically studied the interaction of steady uniform flow of a magnetized compressible plasma with an obstacle body of a cylindrical shape. It was found that this process leads to the periodic generation of Alfvénic vortices, which form a characteristic von Kármán street. The Strouhal number is about 0.2 for a broad range of the speeds and the ratios of the gas and magnetic pressures in the plasma. Thus, as in hydrodynamics, the Strouhal number is a robust feature of the considered phenomenon in the case of rarified (e.g., space, astrophysical, and laboratory) plasmas and can be used for plasma diagnostic. First of all, it justifies the possibility of the excitation of transverse oscillations of plasma loops in the solar corona by external upflows [12].

Also, the independence of the vortex shedding period upon the macroscopic plasma parameters (the magnetic field, density, temperature, and the plasma beta), opens up interesting opportunities for the observational determination of the flow speed, e.g., in planetary magnetospheres and in the corona.

The generated vortices are essentially compressible, with the mass density perturbation up to 50%–70% of the ambient value. The mass density perturbation in the vortices is accompanied by the perturbation of a similar strength of the absolute value of the magnetic field. Both mass density and magnetic field perturbations have a shape of filamentary spiral arms. The induced electric current has a similar structure. The steep gradients of the current density

in the generated vortices are the preferential sites for magnetic reconnection and charged particle acceleration, and hence have implications for plasma heating, cross-field transport and EM wave emission. Investigation of these phenomena require modification of the model and will be a subject to a follow-up study.

M.G. is supported by Newton International grant No. NF090143. T. V. D. acknowledges funding from the EC FP7 (FP7/2007-2013) under grant agreement number 220555.

\*M.Gruszecki@warwick.ac.uk

- [1] D. J. Tritton, *Physics of Fluid Dynamics* (Van Nostrand, Princeton, 1977), 1st ed.
- [2] C. H. K. Williamson, *Annu. Rev. Fluid Mech.* **28**, 477 (1996).
- [3] V. Dousset, A. *et al.*, *Phys. Fluids* **20**, 017104 (2008).
- [4] A. Y. Aydemir, *Phys. Plasmas* **12**, 062503 (2005).
- [5] E. Ott, *J. Geophys. Res.* **83**, 2066 (1978).
- [6] T. Emonet *et al.*, *Astrophys. J.* **549**, 1212 (2001).
- [7] J. D. Huba, *J. Geophys. Res.* **101**, 24 855 (1996).
- [8] J. E. Borovsky, *Phys. Plasmas* **13**, 056505 (2006).
- [9] T. W. Jones *et al.*, *Astrophys. J.* **512**, 105 (1999).
- [10] O. Alexandrova *et al.*, *J. Geophys. Res.* **111**, A12 208 (2006).
- [11] C. Foullon *et al.*, *J. Geophys. Res.* **113**, A11 203 (2008).
- [12] V. M. Nakariakov *et al.*, *Astron. Astrophys.* **502**, 661 (2009).
- [13] Z. A. Kereselidze *et al.*, *Geomagnetizm i Aeronomiya* **27**, 165 (1987).
- [14] L. D. Landau *et al.*, *Electrodynamics of continuous media* (Butterworth-Heinemann, Washington, DC, 1984), 2nd ed.
- [15] T. Arber *et al.*, *J. Comput. Phys.* **171**, 151 (2001).
- [16] D. S. Balsara *et al.*, *J. Comput. Phys.* **149**, 270 (1999).
- [17] T. Van Doorselaere *et al.*, *Astrophys. J.* **676**, L73 (2008).